The Use of Damping Based Semi-Active Control Algorithms in the Mechanical Smart-Spring System

Wander Gustavo Rocha Vieira[1]
Department of Aeronautical Engineering,
Sao Carlos School of Engineering,
University of Sao Paulo,
Avenida Joao Dagnone, 1100,
Sao Carlos 13563-120, Sao Paulo, Brazil
e-mail: wander.vieira@usp.br

Fred Nitzsche
Department of Mechanical and
Aerospace Engineering,
Carleton University,
1125 Colonel By Drive ME3135,
Ottawa, ON K1S 5B6, Canada
e-mail: fred_nitzsche@carleton.ca

Carlos De Marqui, Jr.
Department of Aeronautical Engineering,
Sao Carlos School of Engineering,
University of Sao Paulo,
Avenida Joao Dagnone, 1100
Sao Carlos 13563-120, Sao Paulo, Brazil
e-mail: demarqui@sc.usp.br

In recent decades, semi-active control strategies have been investigated for vibration reduction. In general, these techniques provide enhanced control performance when compared to traditional passive techniques and lower energy consumption if compared to active control techniques. In semi-active concepts, vibration attenuation is achieved by modulating inertial, stiffness, or damping properties of a dynamic system. The smart spring is a mechanical device originally employed for the effective modulation of its stiffness through the use of semi-active control strategies. This device has been successfully tested to damp aeroelastic oscillations of fixed and rotary wings. In this paper, the modeling of the smart spring mechanism is presented and two semi-active control algorithms are employed to promote vibration reduction through enhanced damping effects. The first control technique is the smart-spring resetting (SSR), which resembles resetting control techniques developed for vibration reduction of civil structures as well as the piezoelectric synchronized switch damping on short (SSDS) technique. The second control algorithm is referred to as the smart-spring inversion (SSI), which presents some similarities with the synchronized switch damping (SSD) on inductor technique previously presented in the literature of electromechanically coupled systems. The effects of the SSR and SSI control algorithms on the free and forced responses of the smart-spring are investigated in time and frequency domains. An energy flow analysis is also presented in order to explain the enhanced damping behavior when the SSI control algorithm is employed.
[DOI: 10.1115/1.4038034]

1 Introduction

Semi-active control has been gaining prominence in the recent years in order to reduce vibrations in several fields of engineering. As described by different review articles in the field of civil and mechanical engineering [1–3], the focus of the semi-active control is to reduce the forced response of skyscrapers excited by earthquakes [4], to reduce wind induced vibration in bridges [5], and to reduce vibration in road vehicles [6–10]. In semi-active concepts, the vibration is suppressed by modulating the stiffness [11–14], damping or inertial properties of a dynamic system. In contrast to direct-active approaches, the power requirements are relatively low because the actuator forces are not used to directly counteract the vibratory motion. In most devices designed for semi-active control, the work done by the actuator forces is independent from the work done by the excitation forces that are the objective of control [15].

Practical implementation of semi-active approaches includes the use magnetostrictive materials [16], dry friction [17], controllable orifice dampers, and electrorheological or magneto-rheological fluids. The capability of magneto-rheological and electrorheological fluid dampers and variable orifice dampers to achieve significant control of structural damping characteristics has been well established [18,19]. However, somewhat less attention has been given to the development of mechanical devices capable of achieving effective control of structural properties in order to attenuate vibration. One example is the patented smart spring device [20]. The smart spring is a mechanical device capable of achieving effective modulation of its stiffness through the use of semi-active control strategies. The controlled change of the smart spring mechanical impedance has been investigated both experimentally [21,22] and numerically [23] for reducing vibration in fixed and rotary wing aircraft. Significant suppression of vibrations transferred from the rotating wing system of a helicopter to the nonrotating system is reported in the literature [24]. An independent study also showed that the controlled modulation of the stiffness at the root of a helicopter blade could result in significant reduction of vibration energy at target frequencies [25]. More recently, Nitzsche et al. [26] report the successful experimental attenuation of vibrations at a specific frequency (2/rev) by using the smart spring associated with a dynamically and geometrically scaled helicopter blade during whirl tower tests.

An important feature of each semi-active system for vibration reduction of mechanical structures is the control law. Some of control algorithms are defined in different physical domains, such as the synchronized switch damping (SSD) semi-passive control [27,28], the resetting techniques [29–31], as well as the skyhook control law [32,33]. The SSD scheme leads to semi-passive control of electromechanically coupled structures by using a switching circuit. The piezoelement is intermittently switched from open circuit to a specific electrical boundary condition (short circuit in the synchronized switch damping on short case or resonant circuit in the synchronized switch damping on inductor case) synchronously with mechanical displacement, and, therefore, the voltage output of the piezoelectric material is in phase with structural velocity, leading to enhanced dissipation along each cycle of oscillation [34].

Bobrow et al. [29] employ a resetting semi-active technique to a mechanical-hydraulic system. The device is a double acting hydraulic cylinder whose rods (and consequently pistons) are connected to a host structure. A valve (that is originally closed) connects both sides (chambers) of the cylinder. Since the host structure is oscillating, the mechanical-hydraulic system acts as spring element (while the valve is closed), which is able to store energy by compressing the air as the piston is displaced. The valve is opened (and closed as soon as possible) when the piston velocity is zero, resetting the system to its original stiffness and leading

[1]Corresponding author.

Contributed by the Technical Committee on Vibration and Sound of ASME for publication in the Journal of Vibration and Acoustics. Manuscript received March 8, 2017; final manuscript received September 8, 2017; published online October 20, 2017. Assoc. Editor: Lei Zuo.

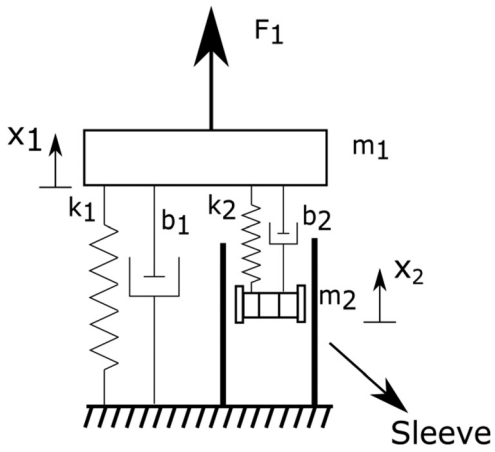

Fig. 1 Smart spring concept

to energy dissipation. Later, Jabbari and Bobrow [30] extend the mechanical-hydraulic analysis reported in Ref. [31] to a pneumatic cylinder. Variations of such systems are reported [35,36]. In general, the resettable devices are employed to attenuate vibrations caused by wind loads or seismic excitations in civil structures.

It is interesting to note that, although developed for different applications as well as different frequency ranges (when compared to the resettable devices), the synchronized switch damping on short (SSDS) technique is quite similar to the resetting semi-active technique discussed in the previous paragraph [29]. In the SSDS, the piezoelement is kept in open circuit condition until an extremum of displacement is detected. At this stage, the system is switched to short circuit condition until voltage is canceled (when is reswitched to open circuit and so on). Both techniques (SSDS and resetting semi-active technique) are employed in this work to obtain the smart-spring resetting (SSR) control technique to be employed in the smart spring device (that will be later discussed). By using a force-voltage analogy (presented in the Appendix of this paper), one can note that typical force waveform of the SSR case is analog to the typical voltage waveform of the SSDS case. The smart-spring inversion (SSI) technique, also discussed in the present work, is based on the synchronized switch damping on inductor (SSDI). In the SSDI case, the voltage is inverted when the piezoelement is quickly connected to an inductor, resulting in a mechanical dissipative force acting along each cycle of oscillation (voltage in phase with mechanical velocity due to switch) and, consequently, mechanical dissipation. The analogy between an electromechanical case and the mechanical system investigated in this work is also presented in the Appendix of this paper, showing that the SSI technique is similar to the SSDI technique (although employed in different physical domains).

In this work, the governing equations of the smart spring mechanical system as well as its operation principle are presented. Although the smart spring has been originally employed for stiffness modulation, in this work, the semi-active control algorithms SSR and SSI are employed for damping enhancement. The control performance of each control algorithm (SSR and SSR) to damp the free response and the forced response of the smart spring is discussed. Moreover, an energy flow analysis is presented in order to explain and to quantify the control performance of the smart spring using the SSR and SSI techniques.

2 The Smart-Spring Modeling

The smart-spring mechanism displayed in Fig. 1 consists of two mass-spring-damper systems arranged in parallel. In this work, these two mass-spring-damper systems are named as load paths. The system denoted with subscript 1 is called main load path, where the spring k_1 and damper b_1 connect the mass m_1 to the ground. The mass-spring-damper system denoted with subscript 2 is called auxiliary load path, where the spring k_2 and damper b_2 connect the mass m_2 to the mass of the main load path. The auxiliary load path can be connected/disconnected by the action of an applied voltage at the terminals of a piezoelectric stack (mass m_2 in Fig. 1) that results in contact between the piezoelectric material and the sleeve at the ground, generating friction force and ultimately engagement. An advantage of the smart-spring is the low energy consumption. One can see that the expansion direction of the piezoelectric stack is orthogonal to the motion direction of both main and auxiliary load paths. Therefore, no energy is added to the system by the piezoelectric stack electrical actuator since it does not perform work, although energy is required to actuate the piezoelectric element.

Three different states can be identified during the operation of the smart-spring. The first state occurs when the auxiliary path is completely disengaged from the sleeve. In such case, the auxiliary load path works as a mechanical vibration absorber connected to the main load path. In the second state slippage occurs between the piezoelectric stack and the sleeve and a dynamic friction force is present in the system. Finally, in the third state, the second load path (or the stack) is perfectly engaged to the sleeve. In the third condition, since the mass of the auxiliary path is engaged to the sleeve, the effect is to increase the resultant stiffness of the system. The modeling of each state of the smart spring behavior is presented in this section.

Figure 2 shows the free body diagram regarding each load path for different states of the system. The main load is presented in Fig. 2(*a*). The different conditions for the auxiliary load path are described in Figs. 2(*b*)–2(*d*). In particular, Fig. 2(*b*) describes the auxiliary load path when no friction force is present in the system

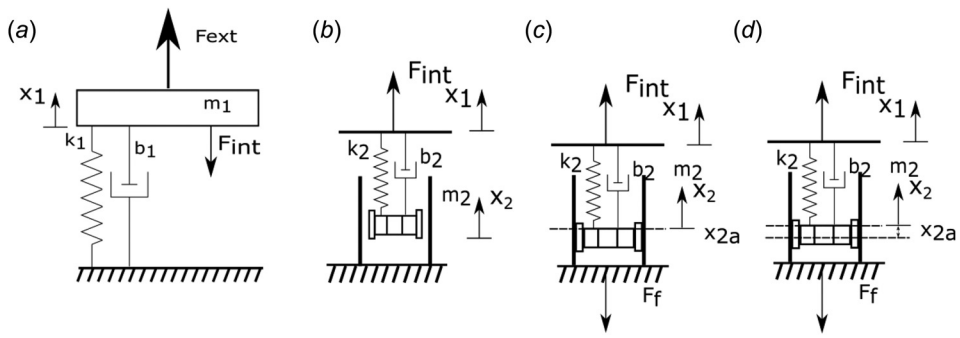

Fig. 2 Free body diagram of the main load path of the smart-spring (*a*) and free body diagram for the auxiliary load path in three different states: disengaged (*b*), auxiliary load partially engaged (*c*), and (*d*) fully engaged

(system fully disengaged), Fig. 2(*c*) shows the auxiliary load path when a dynamic friction force is present in the system, and Fig. 2(*d*) shows the auxiliary load path when a static friction force is present in the system (fully engaged).

The general equation of motion for the main load path can be written as

$$m_1\ddot{x}_1 + b_1\dot{x}_1 + k_1x_1 - F_{\text{int}} = F_{\text{ext}} \tag{1}$$

where x_1 is the displacement of the main load path, and F_{ext} is the external force applied to the main load path. F_{int} is the internal force in the main load path due to the auxiliary load path, which is described as

$$F_{\text{int}} = k_2(x_1 - x_2) + b_2(\dot{x}_1 - \dot{x}_2) \tag{2}$$

where x_2 is the displacement of the auxiliary load path.

The general equation of motion for the auxiliary load path when there is motion at the secondary load path is given as

$$m_2\dot{x}_2 + b_2(\dot{x}_2 - \dot{x}_1) + k_2(x_2 - x_1) = F_f \operatorname{sgn}(\dot{x}_2) \tag{3}$$

where F_f is the friction force. Equation (3) can include the modeling of the state 2, when a dynamic friction force acts in at the auxiliary load path, and also can be employed to model the state 1 that is characterized by the absence of friction force (F_f is zero) in the auxiliary load path (the system is disengaged).

The governing equations of the smart-spring for the state 2, when a dynamic friction force acts in the auxiliary load path, are obtained by combining Eqs. (1)–(3) resulting

$$\begin{aligned} m_1\ddot{x}_1 + b_1\dot{x}_1 + b_2(\dot{x}_1 - \dot{x}_2) + k_1x_1 + k_2(x_1 - x_2) &= F_{\text{ext}} \\ m_2\ddot{x}_2 + b_2(\dot{x}_2 - \dot{x}_1) + k_2(x_2 - x_1) &= F_f \operatorname{sgn}(\dot{x}_2) \end{aligned} \tag{4}$$

that can also employed to describe the behavior of the system in the absence of friction force ($F_f = 0$) in the auxiliary load path, resulting in the state 1 (load paths of the smart spring disengaged). Thus, the governing equations for the smart-spring can be written as

$$\begin{aligned} m_1\ddot{x}_1 + b_1\dot{x}_1 + b_2(\dot{x}_1 - \dot{x}_2) + k_1x_1 + k_2(x_1 - x_2) &= F_{\text{ext}} \\ m_2\ddot{x}_2 + b_2(\dot{x}_2 - \dot{x}_1) + k_2(x_2 - x_1) &= 0 \end{aligned} \tag{5}$$

when the state 1 is considered.

It is also important to consider the state 3, when the load paths of the smart spring are perfectly engaged. In such case, mass m_2 is perfectly engaged to the sleeve due to a static friction force (absence of relative motion between the mass of the auxiliary load path and the ground). It is important to highlight that, in this work, the sleeve is assumed long enough to allow perfect engagement in different positions of x_2. Therefore, the velocity and acceleration of the mass of the auxiliary load path are zero and the smart-spring can be described by only one equation. This single equation is the governing equation of the main load path with a modified F_{int} term. In such case F_{int} is rewritten as

$$F_{\text{int}} = k_2(x_1 - x_{2a}) + b_2\dot{x}_1 \tag{6}$$

that when included in the governing equation of the main load path (Eq. (1)) results

$$m_1\ddot{x}_1 + (b_1 + b_2)\dot{x}_1 + (k_1 + k_2)\dot{x}_1 - k_2x_{2a} = F_{\text{ext}} \tag{7}$$

which is the governing equation for state 3. In such case, the maximum static friction force should be higher than F_{int} in order to avoid an undesirable sliding between the ground and the mass m_2.

3 Semi-Active Control Algorithms

After introducing the modeling of each state of the smart-spring, this section presents the semi-active control algorithms that are employed in this work. It is important to note that the goal of each control algorithm is vibration attenuation of the main load path of the smart spring (that should be connected to a host structure for vibration attenuation). In the Appendix, a mechanical equivalent model of a single-degree-of-freedom (SDOF) electromechanically coupled system is presented by using a force-voltage analogy. By using the mechanical equivalent model, it is shown that the smart spring is similar to the SDOF electromechanically coupled system. Therefore, it is also shown that the SSR and SSI techniques to be described in Secs. 3.1 and 3.2 are similar to the SSDS and SSDI techniques that have been discussed in Sec. 1 and also modeled and analyzed in the literature [27,28,37–39]. This way, due to the similarities with the electromechanical control cases, the SSR and SSI cases of the smart spring are only briefly discussed. Here, it is worth mentioning that both semi-active control algorithms applied to the smart-spring in this work require that the frequency of the auxiliary load path should be greater than that of the main load path.

3.1 Smart-Spring Resetting. The basis of this algorithm is to reset the relative displacement between the main and auxiliary load paths (unloading the spring of the secondary load path and, consequently, resetting the force of the spring of the secondary load path) wherever there is an extremum of the displacement of the main load path. It is interesting to note the similarity with the SSDS case where voltage is canceled when displacement reaches a maximum (and a force-voltage analogy is employed in this work). Figure 3 show the SSR semi-active control algorithm applied to the smart-spring. Figure 3 is not based on simulations and is only qualitative information to support the discussion.

The natural condition of the smart-spring is assumed in this work as the auxiliary load path is engaged to the sleeve (ground) and the spring of the auxiliary load path is unloaded (Fig. 3-1). This condition refers to the state 3 presented in Sec. 3. In such condition, the system is governed by Eq. (7). Figures 3-1 and 3-2 show that the mass of the main load path is moving upward while the displacement of the auxiliary path does not change (since the system is engaged). In such case, the spring of the auxiliary load path (as well as of the main load path) is being loaded (increasing elastic potential energy). In the extremum of displacement of the main load path (Fig. 3-2), the springs of both load paths are loaded. At this stage, voltage is applied to the piezoelectric stack in order to release the auxiliary load path (Fig. 3-3). During the disengagement of the auxiliary load path (before the system is fully disengaged), friction force between the sleeve and the auxiliary load path mass is observed. It is important to mention that because there is a velocity difference between the auxiliary load path and the sleeve, the nature of the force is dynamic. This condition is governed by Eq. (4). Later, the auxiliary load path is fully disengaged (no friction force between auxiliary load path mass and the sleeve), resulting in the state 2 discussed in Sec. 2. The smart-spring is then governed by the Eq. (5). The mass of the auxiliary load path moves upwards and this condition is kept until the auxiliary load spring deformation is zero (fully unloading the spring or resetting the spring, what is shown in Figs. 3-3 and 3-4) when the system is again engaged. The duration of this time interval (unloading or resetting) is one quarter of the period of the auxiliary load path (as observed in the SSDS case). Figure 3-4 shows that when the main load path reaches a minimum the spring has been again loaded (due compression) and voltage is again applied to the piezostack releasing the auxiliary path (Fig. 3-5). Then, the system again engaged when the spring is unloaded (Fig. 3-6). During the engagement a dynamic friction force between the sleeve and the auxiliary load path mass is observed causing dissipation. This condition is governed by Eq. (4). When the system is fully engaged, the state 1 described in Sec. 2 is again achieved.

Therefore, elastic potential energy is stored in the springs when the load paths are engaged, then the system is reset (to a low stiffness condition due to disengagement) and energy is dissipated during the transitions. It is important to note that although

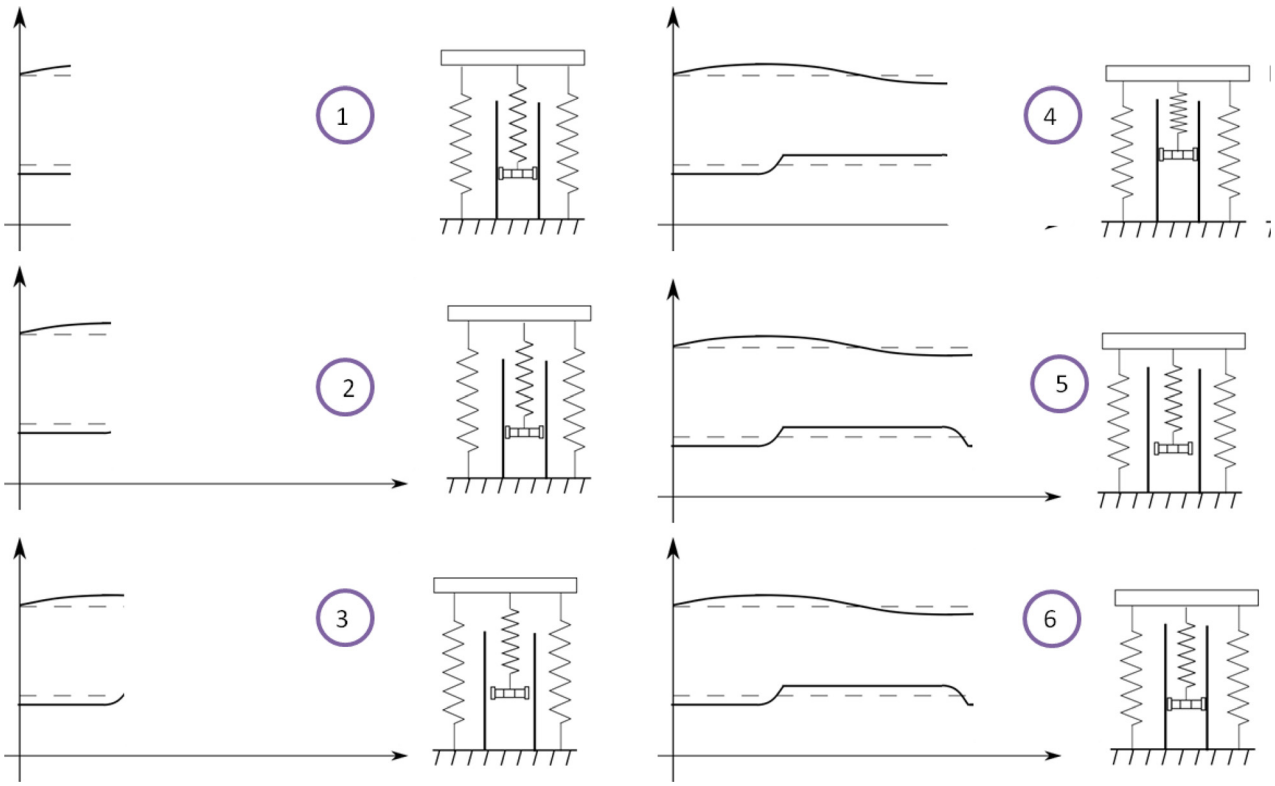

Fig. 3 Detailing of the SSR auxiliary load path releasing/engaging dynamics

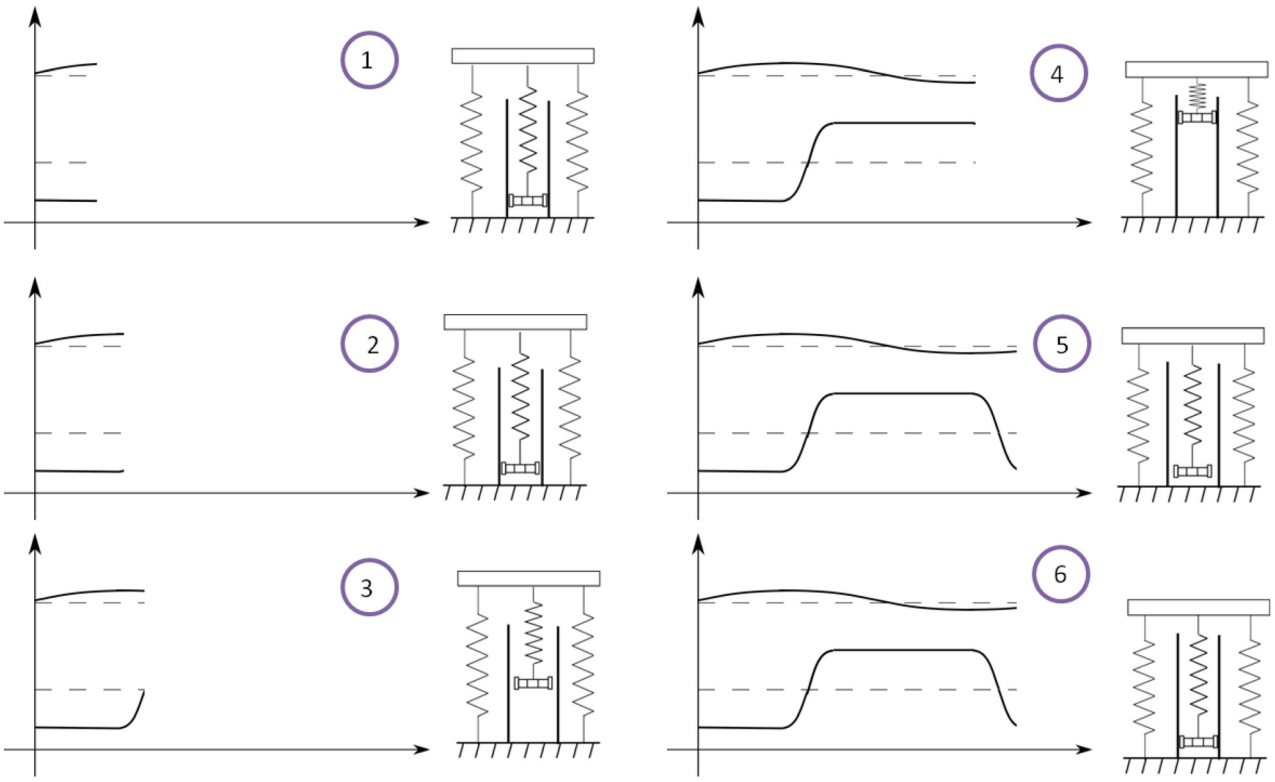

Fig. 4 Detailing of the SSI auxiliary load path releasing/engaging dynamics

dissipation occurs during the transitions, the reason for damping enhancement of the smart spring is the modified phase between the force of the spring of the auxiliary load path and the velocity of the main load path due to the engagement–disengagement process (as will be shown in Sec. 4). Therefore, since the SSR is similar to the resetting control discussed in Sec. 1 that is also similar to the SSDS case also discussed in Sec. 1 and in the Appendix, the wave forms of the force of the spring of the auxiliary load path is similar to the wave forms of the voltage in the SSDS case (as provided in the Appendix).

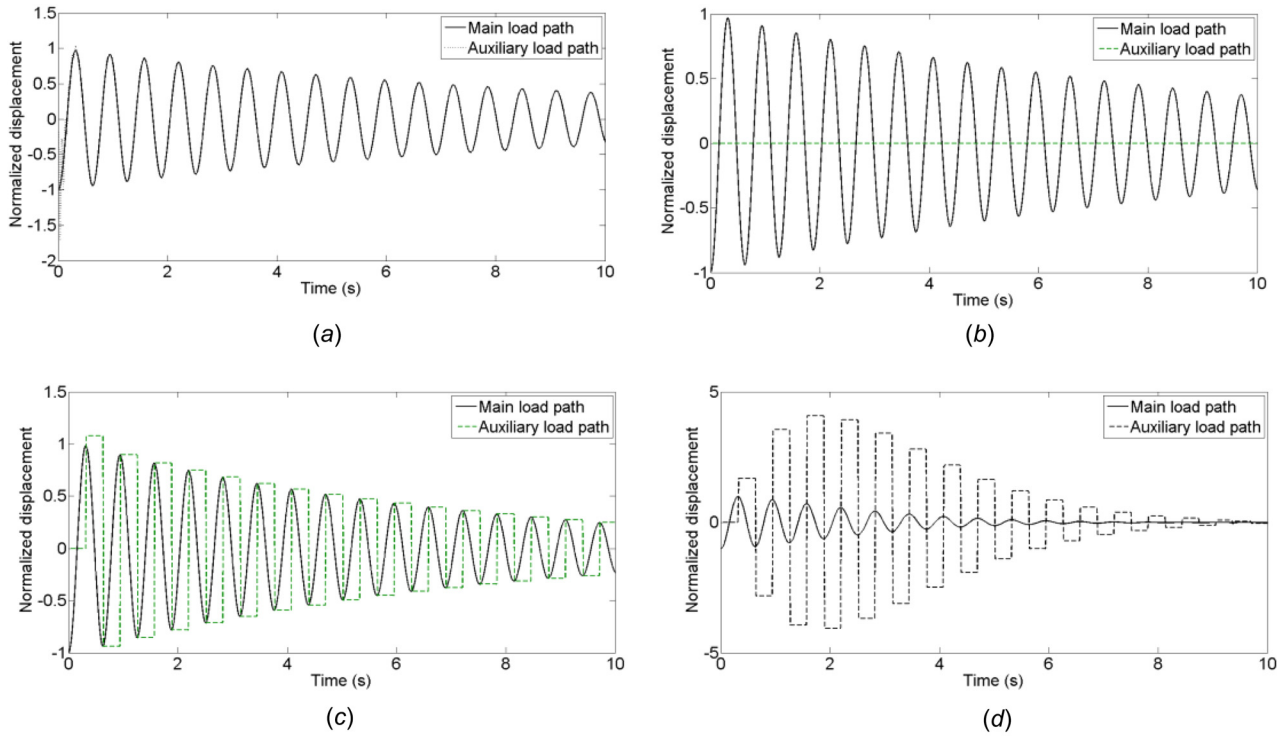

Fig. 5 Free response of the smart-spring using the equivalent switching procedures for the (*a*) soft configuration, (*b*) hard configuration, (*c*) SSR, and (*d*) SSI

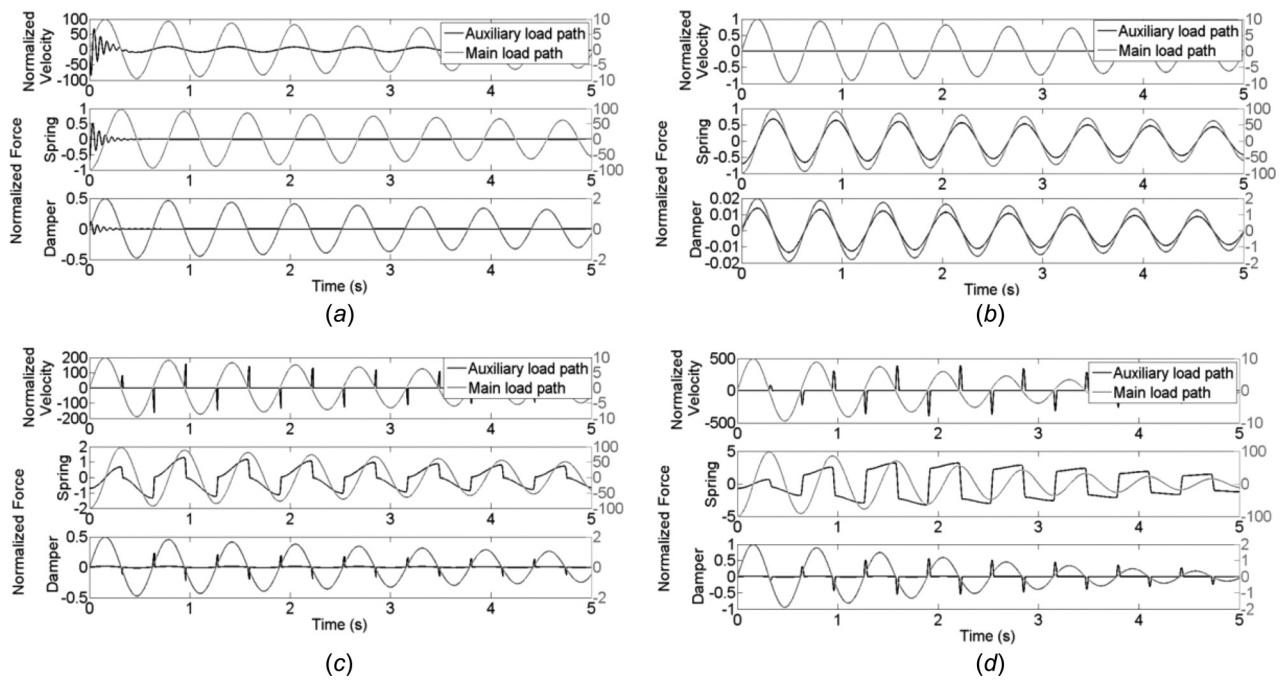

Fig. 6 Time histories of the forces on the smart spring system for the (*a*) soft configuration, (*b*) hard configuration, (*c*) SSR, and (*d*) SSI

3.2 Smart-Spring Inversion. The SSI semi-active control technique is presented in this section. The basis of this algorithm is to allow the inversion of the force of the spring of the auxiliary load path (or the inversion of relative displacement between the load paths) wherever there is an extremum of the displacement of the main load path. Figure 4 shows the SSI semi-active control algorithm applied to the smart spring.

The natural condition of the smart-spring is assumed in this work as the auxiliary load path is engaged to the sleeve (ground) and unloaded (Fig. 4-1). This refers to the state 3 discussed in Sec. 2. In such condition, the system is governed by Eq. (7). In the extremum of displacement of the main load path, the springs of both load paths store energy (Fig. 4-2). At such condition, voltage is applied to the piezoelectric stack in order to release the

auxiliary load path (Fig. 4-3). The auxiliary load path is fully disengaged (no friction force between auxiliary load path mass and the sleeve), resulting in the state 2 discussed in Sec. 2. The smart-spring is then governed by the Eq. (5). This condition is kept until the force of the auxiliary load spring is inverted. The duration of this time interval is half of the auxiliary load path period. Note that the velocity of the auxiliary load path is almost zero (Fig. 4-4). At this point, no voltage is applied to the piezostack (Fig. 4-4) and during the engagement a dynamic friction force between the sleeve and the auxiliary load path mass is observed. This condition is governed by Eq. (4). However, one should note that the duration of this interval is very small in comparison with the SSR case and the energy loss could be neglected. Later, when the main load path reaches a minimum (Figs. 4-4 and 4-5), the auxiliary load path is again released (Fig. 4-5) until the force of the spring of the auxiliary load path is inverted (Fig. 4-5). Then, the system is fully engaged and the state 1 described in Sec. 2 is achieved again.

Therefore, energy is stored in the springs when the load paths are engaged, then the system is set to a low stiffness condition (disengaged) and the force related to the spring of the auxiliary path inverted, when the full engagement is achieved again. Thus, the SSI is quite similar to the to the SSDI case also discussed in Sec. 1 and in the Appendix. In this case, there is also a phase modification between force of the spring of the auxiliary path and velocity of the main load path. Since they are in phase during most of each cycle of oscillation due to the switch process), enhanced damping is verified in the smart spring. The wave forms of spring force are shown in the Appendix and will also be discussed in Sec. 4.

4 Results

In this section, the effects of the SSR and SSI control strategies on the behavior of the smart spring are presented and compared in the time and in the frequency domains. The results were obtained by solving the equations that govern the smart spring (presented and discussed in Sec. 2). A time-domain integration scheme based on a time finite difference method with variable step to simulate the behavior of the system when different conditions are experienced (i.e., a small time-step is used when a dynamic friction acts on the model). The engagement and disengagement of the piezoelectric stack to the sleeve is performed according to the discussion presented in Sec. 3. First, the time histories of the displacement of each load path are presented for a free vibration condition. In the free response analysis, an initial condition on the displacement was assumed. The phase shift and amplitudes of the forces applied in the main load path mass are compared between the soft and hard case and the semi-active cases are considered. Moreover, an energy flow analysis of each element of the smart spring is presented in order to explain the performance of each semi-active control technique applied to the smart spring for damping enhancement. Next, the performance on vibration reduction of each control strategy is presented in the frequency domain for a forced vibration condition. In the frequency domain analysis, an external harmonic forcing term was used (initial conditions set to zero) and the steady-steady displacement amplitude value was obtained for each investigated frequency value by using the time-domain integration. The parameters employed in the simulations are shown in Table 1.

Table 1 Smart-spring parameters

Parameter	Value
Auxiliary to main load path stiffness ratio	0.7%
Auxiliary to main load path frequency ratio	20
Damping coefficient of the main load path	1%
Damping coefficient of the auxiliary load path	10%
Excitation force by main path mass	Unitary

4.1 Free Vibration Response. Figure 5 displays the normalized displacement (by the initial displacement considered in the main load path) when a unitary initial condition applied to both load paths (the initial velocities are zero) when the soft case (Fig. 5(*a*)), the hard case (Fig. 5(*b*)) as well as the SSR (Fig. 5(*c*)) and SSI (Fig. 5(*d*)) cases are considered. Initially, it is worth to discuss the soft and hard cases. In the soft case of Fig. 5(*a*), the mass of the auxiliary load path is totally disengaged (i.e., the mass is free to oscillate) from the ground (sleeve of Fig. 1). Then it is seen that the auxiliary load path mass oscillates with a fast decaying due to the relatively high damping ratio related to the damper of the auxiliary load path. In the hard case the mass of the auxiliary load path is totally engaged to the sleeve (i.e., there is no motion of this mass). Then, Fig. 5(*b*) shows that the displacement of the auxiliary load path is always zero. Moreover, the equivalent stiffness is obtained from the combination of the main and auxiliary load path stiffness. Therefore, in the soft case, the mass of the main load path oscillates in a frequency obtained from the square root of the stiffness of the main load path to the mass of the main load path ratio while in the hard case the mass of the main load path oscillates in a frequency slightly larger than the one of the soft case since the equivalent stiffness is larger (than in the soft case).

For the SSR case in Fig. 5(*c*), when the displacement extremum of the auxiliary path is detected, the main and auxiliary paths are engaged; when the force of the spring of the auxiliary path is zero, the stack is disengaged. A similar procedure is taken in Fig. 5(*d*). However, in such case, the paths are engaged until the complete inversion of the force of the spring of the auxiliary load path occurs. The vibration reduction in the main path is the control objective. It is clear that vibration attenuation is more pronounced in Fig. 5(*d*) (SSI) than in Fig. 5(*c*) (SSR). After 10 s, the amplitude of the main load path is reduced by 18% in Fig. 5(*c*) and by 75% in Fig. 5(*d*). The inversion of the force of the auxiliary load path causes an interesting phenomenon. One should also note in Fig. 5(*d*) that the amplitude of motion of the auxiliary load path increases in the first initial seconds of simulation and later decreases. When the SSI technique is employed, more energy is transferred from the main load path to the auxiliary load path (more detailed discussion will be provided in Fig. 10). However, it is seen that after a few cycles the ratio between the displacement of the main and auxiliary load paths remains almost constant. Since more dissipation is also achieved (when compared to the SSR case), the amplitude of motion of the auxiliary load path (as well as of the main load path) decays along time.

Figures 6(*a*)–6(*d*) show the velocity and forces that acts on the mass of the main load path for the soft and hard cases (secondary load path disengaged and engaged, respectively) and SSR and SSI cases, respectively. The figure displays the velocity, main load path spring force, auxiliary load path spring force, main load path damper force, and auxiliary load path damper force. A first glance on the velocity plot shows that the vibration is reduced when the semi-active cases are employed (in comparison soft and hard cases). One should note that the phase between the spring force of the auxiliary load path (due to k_2) and the velocity of the main load path is 90 deg in Fig. 6(*b*). Therefore, dissipation occurs only during part of one cycle of oscillation. On the other hand, the semi-active cases adjusts the phase between spring force and velocity (as well as amplify the forces in the auxiliary load path elements) and, therefore, enhances the energy dissipation. Moreover, a further increase in the force amplitude is seen in the SSI case (compared with the SSR case), resulting in more energy dissipation from the main load path.

A qualitative estimation of the instantaneous power for the smart-spring main load path can be obtained through the multiplication of a respective force by the velocity of the mass m_1. The

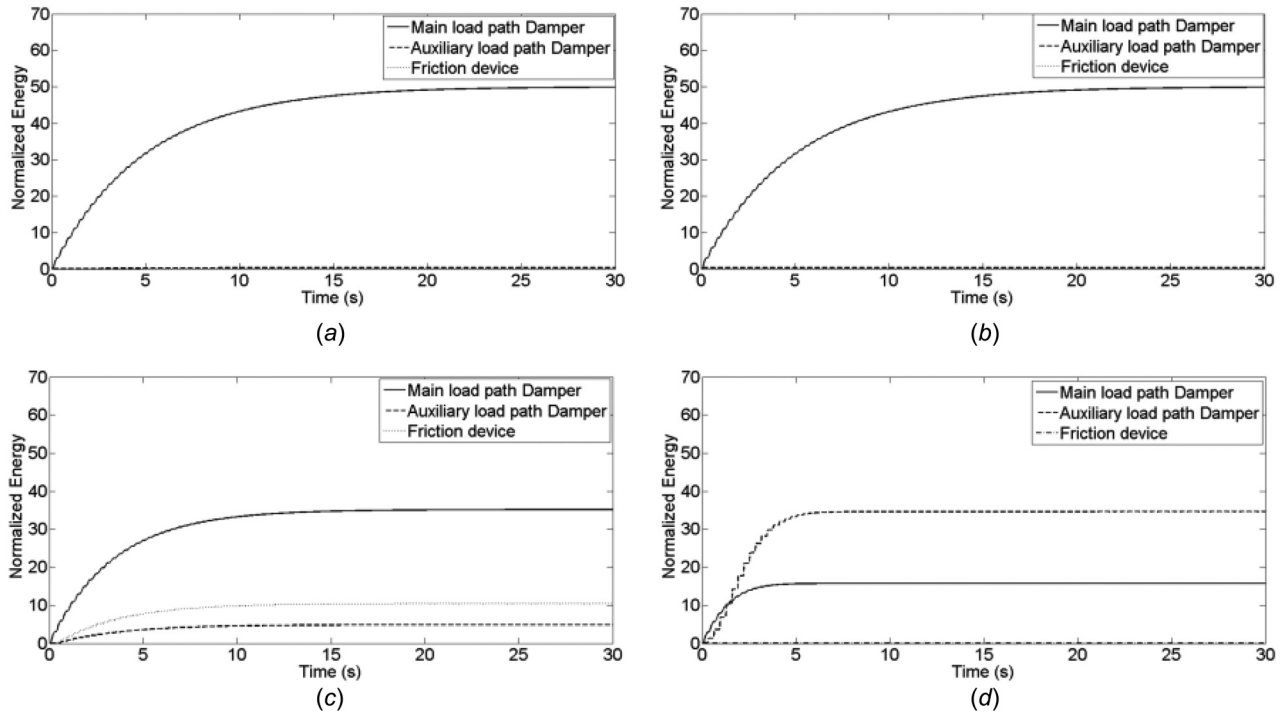

Fig. 7 Energy flow analysis considering the (*a*) soft configuration, (*b*) hard configuration, (*c*) SSR, and (*d*) SSI

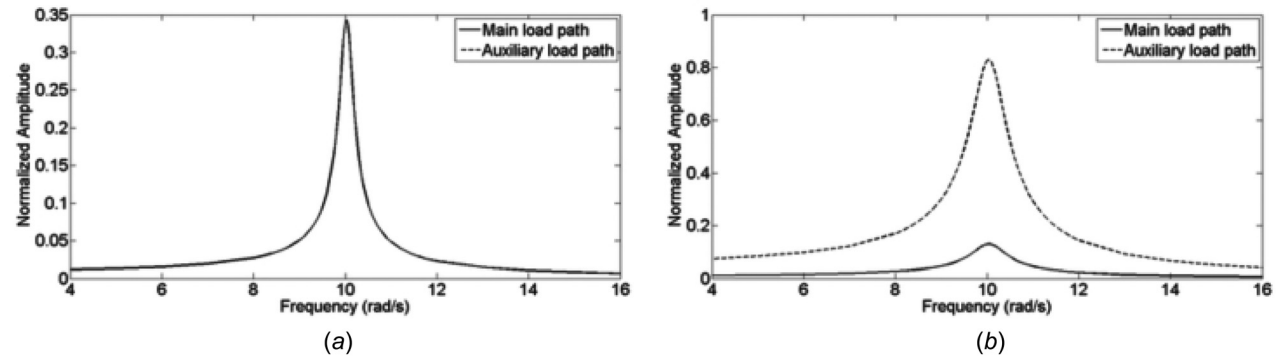

Fig. 8 Harmonic forced response of the smart-spring using the equivalent switching procedures: (*a*) SSR and (*b*) SSI

associated energy is refereed as the time integration of the power. Figures 7(*a*)–7(*d*) show the energy dissipation on the smart-spring for the soft and hard cases and also SSR and SSI configurations. When the soft and the hard configurations are used, the energy is dissipated mainly on the damper of the main load path, and a small portion is dissipated on the auxiliary load path damper. Besides, when the soft and hard configurations are implemented, the friction term does not dissipate energy since the product between friction force and velocity is always equal zero. For the soft case, although the auxiliary load path has velocity different from zero there is no friction force in the system. For the hard case, the auxiliary load path velocity is equal zero although friction force is observed in the system. It is important to say that differently to the soft and hard cases, the damper of the auxiliary load path also dissipates a considerable amount of energy when the semi-active cases are considered since more energy is transferred from the main to the auxiliary load path.

In particular, when the SSI control strategy is used (Fig. 7(*d*)), more energy is dissipated on the damper of the auxiliary load path than in the damper of the main load path. In the end, it is also important to discuss the role of the dissipation of energy promoted by the friction force on the smart-spring in the semi-active case. The friction device dissipates a considerable amount of energy when the SSR strategy is considered (Fig. 7(*c*)). In this configuration, the friction force is switched on when there is a maximum velocity (i.e., zero displacement for the auxiliary load path) and a dynamic friction force acts in the auxiliary load path mass to equalize the mass velocity to the ground. Otherwise, when the SSI control scheme is used no energy is dissipated on the friction device since the friction device is switched on when the auxiliary load path velocity is zero (i.e., a extremum displacement value). One can see that the amount of energy extracted from the main load path to the auxiliary load path increases when the semi-active cases are considered (i.e., the phase of the auxiliary load path is synchronized with the main load path velocity and amplitude of the spring force is increased). Clearly, the dissipated energy is higher when the SSI scheme is considered. In such case, the spring force is larger than in any other cases considered in this work.

4.2 Forced Vibration Response. Figure 8 shows the forced response for the single harmonic excitation due to a unitary F_{ext}/m_1 applied to the main load path over a range of frequencies. In the simulations, the system was excited at each frequency until

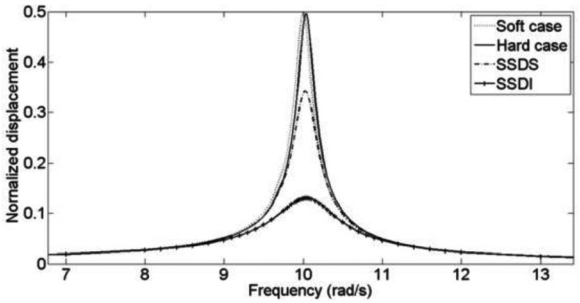

Fig. 9 Harmonic forced response of the main load path of the smart-spring using the SSR, SSI, engaged (hard) and disengaged (soft)

the steady-state condition was achieved; then, next frequency was analyzed and so on. The resonance frequency of the main path is 10 rad/s and the resonance frequency of the auxiliary path is 200 rad/s. The resonance frequency of each DOF is well separated and this should be a design condition for any successful implementation of the smart-spring [26]. As in an electromechanically coupled system using the SSDI strategy, where the resonance frequency of the electrical domain is much higher than that of the mechanical domain, the resonance frequency of the auxiliary path of the smart-spring must be significantly higher than the resonance frequency of the main load path [26].

Figures 8(*a*) and 8(*b*) show the normalized displacement of both load paths when the SSR and SSI switching procedures are considered, respectively. Although the linear spectrum of the auxiliary path is greater in the SSI equivalent case, one should note that the linear spectrum of the main path is substantially smaller in the SSI case than in the SSR case (due to the counteracting mechanical force in the main load path during the switching process, as previously discussed), which is the objective of control.

Figure 9 shows the forced response of the main load path with the smart-spring engaged (hard case), disengaged (soft case) and using the semi-active control strategies. The disengaged resonance frequency of the smart-spring is 10 rad/s (resonance frequency of the main load path) and the engaged resonance frequency is slightly larger since the equivalent stiffness is larger in such case. Since the similarities between the smart spring and a SDOF electromechanically coupled system has been discussed in this paper, one should note that shift in the resonance frequency of the smart spring from the soft to the hard condition is similar to the shift from the short-circuit condition to the open circuit condition in an electromechanically coupled system [40]. As discussed in Fig. 8, the linear spectrum of the normalized displacement of the main load path associated with the SSI control scheme is lower than that of the SSR control scheme due the enhanced damping capabilities introduced by the SSI switching procedure.

5 Conclusions

In this paper, the modeling of the smart spring mechanism is presented. Semi-active control algorithms techniques originally presented for mechanical system, mechanical-hydraulic and electromechanically coupled systems are employed in the smart spring mechanism. This way, in addition to the stiffness modulation previously discussed in the literature, the smart spring is employed in this paper for damping enhancement.

The behavior of the smart spring is investigated in different conditions. First, the free response of the system is discussed for the soft condition, hard, condition and using the SSR and SSI techniques. The shift in the resonance frequency of the main load path of the smart spring from the soft to the hard condition is show to be similar to the shift in the resonance frequency of an electromechanically coupled system from the short circuit to the open circuit condition (since the stiffness of a piezoelectric material is related to the electrical boundary condition). Moreover, the time histories of the forces actuating on the smart spring are also shown. The semi-active control techniques introduce a phase modification that makes the term related to the spring force of the auxiliary load path stiffness dissipative over each cycle of oscillation. Therefore, damping is increased when the semi-active control techniques are employed and the oscillations of the main load path significantly attenuated. Moreover, the attenuation is further increased when the SSI technique is employed, since an amplification of the spring force is also achieved. An energy flow analysis for each case considered in this paper was also presented and the energy dissipation quantified.

In the second case study, the forced frequency response is evaluated for the two control strategies and compared to the engaged (hard) and disengaged (soft) conditions of the smart-spring. The results show that the semi-active control strategies are able to significantly attenuate the response of the main load path. The SSI scheme presents an enhanced performance to reduce vibrations when compared to the SSR scheme under the same conditions. This emphasizes the ability of the smart-spring to control target harmonics of a forced frequency response problem. It is important to remember that in the applications previously reported in the literature, the main load path is connected to a vibratory system (wing or helicopter blade) with the goal of vibration attenuation at target frequencies. The semi-active control techniques are shown to be an effective way to damp oscillations by using the mechanical smart spring system.

Funding Data

- Conselho Nacional de Desenvolvimento Cientifico e Tecnologico (Grant Nos. 232404/2014-3, 401777/2012-0, 402160/2013-4, and 574001/2008-5).
- Fundacao de Amparo a Pesquisa do Estado de Minas Gerais (Grant No. APQ-0076-09).

Nomenclature

b_q = mechanical equivalent damping
b_1 = main load path damping
b_2 = auxiliary load path damping
c_p = piezoelectric capacitance
F_{ext} = external force
F_f = friction force
F_{int} = internal force
k_q = mechanical equivalent stiffness
k_1 = main load path stiffness
k_2 = auxiliary load path stiffness
L = inductor
m_q = mechanical equivalent mass
m_1 = main load path mass
m_2 = auxiliary load path mass
q = mechanical equivalent displacement related to the electrical charge
q_e = electrical charge on piezoelectric
R = resistor
v_p = voltage output
x_1 = main load path displacement
x_2 = auxiliary load path displacement
x_{2a} = auxiliary load path stuck displacement
θ = electromechanical coupling

Appendix: Similarities Between the Synchronized Switch Damping Semipassive Control Techniques and the Smart-Spring Resetting and Smart-Spring Inversion

This Appendix discusses the equivalence between the SSD control techniques (applied to electromechanically coupled systems) and the SSR and SSI techniques applied to the mechanical smart-

spring. Initially, the modeling of a single-degree-of-freedom electromechanically coupled system is presented. Later, an equivalent mechanical model for the SDOF electromechanically coupled system is obtained. This equivalent model shows that the smart spring discussed in this paper can be considered similar to a SDOF electromechanically coupled system. Therefore, control techniques similar to the SSD techniques usually employed in electromechanically coupled systems can be employed in mechanical systems such as the smart spring resulting in similar effects.

Figure 10 displays the schematics of a SDOF electromechanically coupled system associated with a nonlinear switching circuit. The electrical element represented in the circuit of Fig. 10 is a finite inductance that is in series with an electrical switch, resulting in the SSDI technique discussed in the paper. In particular, the switch is represented in this paper by a resistor. When the switch is open, a large resistance is considered (i.e., open-circuit) and when the switch is closed a small resistance is considered (i.e., short-circuit).

The resulting RL circuit of Fig. 10 can be modeled as

$$L\ddot{q}_e + R\dot{q}_e = v_p \tag{A1}$$

where q_e is the electrical charge, L is the inductance, R the resistance, and v_p the voltage output. The governing equations of the SDOF electromechanically coupled system depicted in Fig. 10 (not considering the electrical circuit) are

$$\begin{aligned} m_1\ddot{x}_1 + c_1\dot{x}_1 + k_1x_1 - \theta v_p &= F_1 \\ c_p v_p + q_p + \theta x_1 &= 0 \end{aligned} \tag{A2}$$

where θ is the electromechanical coupling, c_p is the internal capacitance of the piezoelectric element, v_p is the voltage across the electrodes of the piezoelectric material and q_p is the electrical charge output from the piezoelectric element. The over-dot represents the time derivative. By combining Eqs. (A1) and (A2) and multiplying by the electromechanical coupling, one should obtain the following mechanical equivalent equation:

$$m_q\ddot{q} + b_q\dot{q} + k_q(q - x_1) = 0 \tag{A3}$$

where $q = q_p/\theta$. Equation (A3) is the mechanical equivalent model of the electrical equation (Eq. (A2)) of the SDOF electromechanically coupled system combined to the SSDI circuit presented in Fig. 10. The equivalent mass is $m_q = L\theta^2$, the equivalent damping $b_q = R\theta^2$ and the equivalent stiffness $k_q = \theta^2/c_p$. The equivalent mechanical model for Eq. (A2) is obtained by using the definition of q and piezoelectric stiffness k_q into Eq. (A2) and also using Eq. (A3), resulting

$$\begin{aligned} m_1\ddot{x}_1 + c_1\dot{x}_1 + k_1x_1 + k_q(x_1 - q) &= F_1 \\ m_q\ddot{q} + b_q\dot{q} + k_q(q - x_1) &= 0 \end{aligned} \tag{A4}$$

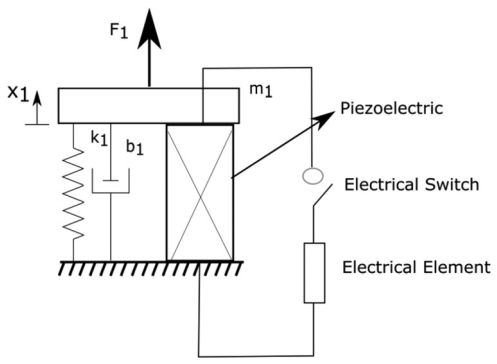

Fig. 10 Schematics of a SDOF electromechanically coupled system combined to a nonlinear switching circuit

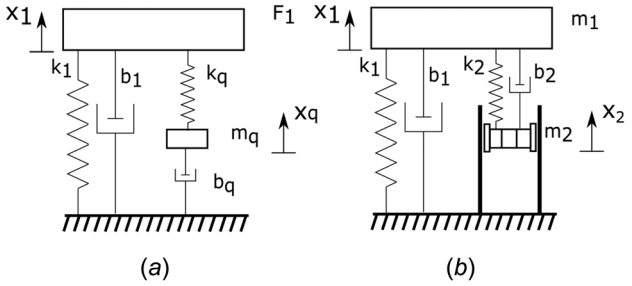

Fig. 11 The comparison between (*a*) the electromechanical system described in a mechanical topology and (*b*) the smart-spring

where the backward coupling θv_p (previously shown in Eq. (A2)) is rewritten in terms of the stiffness related force $k_q(q - x_1)$. Since a switch (R) and an inductor were considered in the electrical domain, Eq. (A4) can be used to describe the SSDI case. On the other hand, the SSDS case can be described Eq. (A4) when $L = 0$ (that results in $m_q = 0$).

Figure 11(*a*) shows the schematic of the mechanical equivalent model while Fig. 11(*b*) shows the smart spring mechanism modeled and discussed in this paper. In Fig. 11(*b*), when the piezoelectric stack of the smart spring (mass m_2 of the auxiliary load path) is perfectly connected to the sleeve the resulting system has maximum stiffness (k_1 is combined to k_2). In the mechanical equivalent model, such condition (switch off or open circuit condition) is obtained in Fig. 11(*a*) when $b_q \to \infty$. The maximum stiffness condition is achieved when the piezoelectric element is in open circuit condition, what is achieved when the switch of the electrical circuit is off. On the other hand, in Fig. 11(*b*), when the stack is not engaged to the sleeve, a second mass-spring system (auxiliary load path) is added to the main load path. One should note in Fig. 11(*a*) that such condition is similar to $b_q = 0$, which is equivalent to the switch on condition in Fig. 10. Therefore, the analysis of the mechanical equivalent model and the analysis of Fig. 11 show that the smart spring can be assumed as a mechanical equivalent system of a SDOF electromechanical system. Moreover, the SSD techniques can also be employed in the smart spring, as will be here discussed.

Figures 12(*a*)–12(*d*) show the phenomenological equivalence of the switching pattern of the displacement for the main and auxiliary load paths of the smart spring using the SSR and SSI control strategies with the semi-passive SSDS and SSDI techniques. The SSDS method is a nonlinear semi-passive technique originally presented by Richard et al. When a local maximum voltage is detected the piezoelement is briefly switched to short circuit condition, canceling the voltage across its electrodes, and reswitched to open circuit condition until the next local maximum voltage (or displacement) occurs. The damping effect results from the energy dissipation during the short circuit phases. The SSDI method is another nonlinear semi-passive method [27,28,37,39,41,42]. In this approach, the switching device is composed of a switch and an external inductance. The switch is briefly closed when a local maximum displacement (or voltage) is detected. At this point, the internal capacitance of the piezoelement and the inductance of the electrical circuit constitute an electrical oscillator. The voltage of the piezoelement is inverted after half period of the electrical oscillator, when the switch is open again [41].

It is important to keep in mind that the SSD techniques, which were first discussed in terms of the behavior of voltage output of the electromechanically coupled system, can be also described in terms of the force related to the spring k_q in the mechanical equivalent system (which connects the main and auxiliary load path) described by Eq. (A4) and in terms of the stiffness of the auxiliary load path (k_2) of the smart spring. When using the SSR technique is employed in the smart spring (Fig. 12(*a*)), the effect of voltage

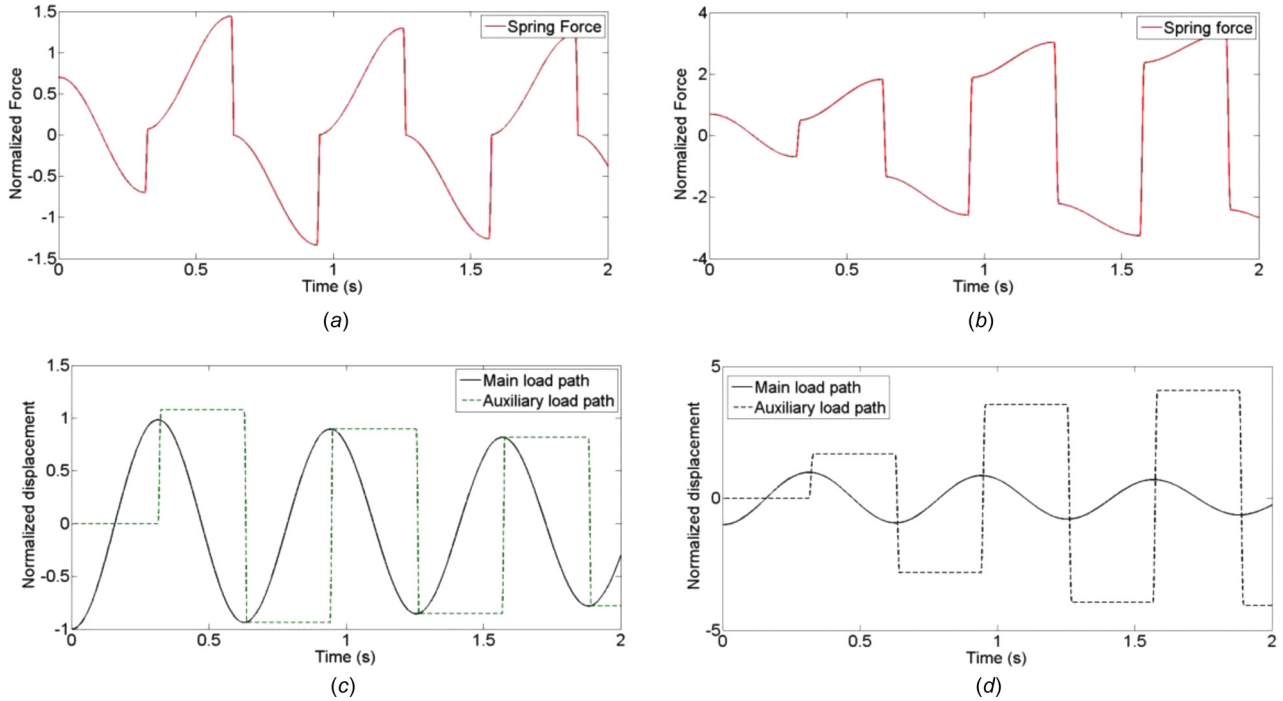

Fig. 12 The switching pattern of the smart spring: force due to the spring k_q for the (*a*) SSDS scheme and (*b*) for the SSDI scheme; the switching pattern for the displacement of the main and auxiliary paths of the smart spring using (*c*) SSDS and (*d*) SSDI schemes

cancelation achieved during the switch on period in the SSDS on the electromechanically coupled system corresponds to the cancelation of spring force of the auxiliary load path. Consequently, by evaluating Eq. (A4), the displacement of the auxiliary load path also presents a nonlinear pattern (Fig. 12(*c*)). On the other hand, when using the SSI technique in the smart spring (Fig. 12(*b*)), the inversion of the force related to k_2 is observed, what corresponds to the inversion of voltage output of piezoelectric element in the SSDI case of the electromechanically coupled SDOF system (always following the analogy assumed in this Appendix). Consequently, by evaluating the Eq. (A4), the displacement of the auxiliary load path also presents a nonlinear behavior as displayed in Fig. 12(*d*).

References

[1] Soong, T. T., and Spencer, B. F., Jr., 2002, "Supplemental Energy Dissipation: State-of-the-Art and State-of-the-Practice," Eng. Struct., **24**(3), pp. 243–259.

[2] Spencer, B. F., Jr., and Nagarajaiah, S., 2003, "State of the Art of Structural Control," J. Struct. Eng., **129**(7), pp. 845–856.

[3] Symans, M. D., and Constantinou, M. C., 1999, "Semi-Active Control Systems for Seismic Protection of Structures: A State-of-the-Art Review," Eng. Struct., **21**(6), pp. 469–487.

[4] Kurata, N., Kobori, T., Takahashi, M., Ishibashi, T., Niwa, N., Tagami, J., and Midorikawa, H., 2000, "Forced Vibration Test of a Building With Semi-Active Damper System," Earthquake Eng. Struct. Dyn., **29**(5), pp. 629–645.

[5] Sahasrabudhe, S. S., and Nagarajaiah, S., 2005, "Semi-Active Control of Sliding Isolated Bridges Using MR Dampers: An Experimental and Numerical Study," Earthquake Eng. Struct. Dyn., **34**(8), pp. 965–983.

[6] Zuo, L., and Zhang, P. S., 2013, "Energy Harvesting, Ride Comfort, and Road Handling of Regenerative Vehicle Suspensions," ASME J. Vib. Acoust., **135**(1), p. 011002.

[7] Fateh, M. M., and Alavi, S. S., 2009, "Impedance Control of an Active Suspension System," Mechatronics, **19**(1), pp. 134–140.

[8] Yao, G. Z., Yap, F. F., Chen, G., Li, W. H., and Yeo, S. H., 2002, "MR Damper and Its Application for Semi-Active Control of Vehicle Suspension System," Mechatronics, **12**(7), pp. 963–973.

[9] Chen, M. Z., Hu, Y., Li, C., and Chen, G., 2016, "Application of Semi-Active Inerter in Semi-Active Suspensions Via Force Tracking," ASME J. Vib. Acoust., **138**(4), p. 041014.

[10] Qin, Y., Zhao, F., Wang, Z., Gu, L., and Dong, M., 2017, "Comprehensive Analysis for Influence of Controllable Damper Time Delay on Semi-Active Suspension Control Strategies," ASME J. Vib. Acoust., **139**(3), p. 031006.

[11] Onoda, J., Endot, T., Tamaoki, H., and Watanabe, N., 1991, "Vibration Suppression by Variable-Stiffness Members," AIAA J., **29**(6), pp. 977–983.

[12] Onoda, J., Makihara, K., and Minesugi, K., 2003, "Energy-Recycling Semi-Active Method for Vibration Suppression With Piezoelectric Transducers," AIAA J., **41**(4), pp. 711–719.

[13] Ledezma-Ramirez, D. F., Ferguson, N. S., and Brennan, M. J., 2011, "Shock Isolation Using an Isolator With Switchable Stiffness," J. Sound Vib., **330**(5), pp. 868–882.

[14] Ledezma-Ramirez, D. F., Ferguson, N. S., and Brennan, M. J., 2012, "An Experimental Switchable Stiffness Device for Shock Isolation," J. Sound Vib., **331**(23), pp. 4987–5001.

[15] Nitzsche, F., 2012, "The Use of Smart Structures in the Realization of Effective Semi-Active Control Systems for Vibration Reduction," J. Braz. Soc. Mech. Sci. Eng., **34**, pp. 371–377.

[16] Krishna, Y., Sarma, B. S., and Shrinivasa, U., 2003, "Shock Isolation Using Magnetostrictive Actuator," Proc. SPIE, **5062**, pp. 270–277.

[17] Ismail, M. I., and Ferguson, N. S., 2017, "Passive Shock Isolation Utilising Dry Friction," Shock Vib., **2017**, pp. 1–21.

[18] Yang, J., Sun, S., Li, W., Du, H., Alici, G., and Nakano, M., 2015, "Development of a Linear Damper Working With Magnetorheological Shear Thickening Fluids," J. Intell. Mater. Syst. Struct., **26**(14), pp. 1811–1817.

[19] Zareh, S. H., Matbou, F., and Khayyat, A. A. A., 2015, "Experiment of New Laboratory Prototyped Magneto-Rheological Dampers on a Light Commercial Vehicle Using Neuro-Fuzzy Algorithm," J. Vib. Control, **21**(15), pp. 3007–3019.

[20] Nitzsche, F., Anant, G., and Zimcik, D., "Structural Component Having Means for Actively Varying Its Stiffness to Control Vibrations," U.S. Patent No. 5,973,440.

[21] Wickramasinghe, V., Chen, Y., and Zimcik, D., 2008, "Experimental Evaluation of the Smart-Spring Impedance Control Approach for Adaptive Vibration Suppression," J. Intell. Mater. Syst. Struct., **19**(2), pp. 171–179.

[22] Yong, C., Zimcik, D. G., Wickramasinghe, V. K., and Nitzsche, F., 2004, "Development of the Smart Spring for Active Vibration Control of Helicopter Blades," J. Intell. Mater. Syst. Struct., **15**(1), pp. 37–47.

[23] Nitzsche, F., Harold, T., Wickramasinghe, V. K., Yong, C., and Zimcik, D. G., 2005, "Development of a Maximum Energy Extraction Control for the Smart-Spring," J. Intell. Mater. Syst. Struct., **16**(11–12), pp. 1057–1066.

[24] Oxley, G., Nitzsche, F., and Feszty, D., 2009, "Smart-Spring Control of Vibration on Helicopter Rotor Blades," J. Aircr., **46**(2), pp. 692–696.

[25] Anusonti-Inthra, P., and Gandhi, F., 2000, "Helicopter Vibration Reduction Through Cyclic Variations in Rotor Blade Root Stiffness," J. Intell. Mater. Syst. Struct., **11**(2), pp. 153–166.

[26] Nitzsche, F., D'Assunção, D., and De Marqui, C., Jr., 2015, "Aeroelastic Control of Non-Rotating and Rotating Wings Using the Dynamic Stiffness Modulation Principle Via Piezoelectric Actuators," J. Intell. Mater. Syst. Struct., **26**(13), pp. 1656–1668.
[27] Richard, C., Guyomar, D., Audigier, D., and Ching, G., 1999, "Semi-Passive Damping Using Continuous Switching of a Piezoelectric Device," Proc. SPIE, **3672**, pp. 104–111.
[28] Richard, C., Guyomar, D., Audigier, D., and Bassaler, H., 2000, "Enhanced Semi-Passive Damping Using Continuous Switching of a Piezoelectric Device on an Inductor," Proc. SPIE, **3989**, p. 288.
[29] Bobrow, J. E., Jabbari, F., and Thai, K., 1995, "An Active Truss Element and Control Law for Vibration Suppression," Smart Mater. Struct., **4**(4), p. 264.
[30] Jabbari, F., and Bobrow, J. E., 2002, "Vibration Suppression With Resettable Device," J. Eng. Mech., **128**(9), pp. 916–924.
[31] Karnopp, D., Crosby, M. J., and Harwood, R. A., 1974, "Vibration Control Using Semi-Active Force Generators," ASME J. Eng. Ind., **96**(2), pp. 619–626.
[32] Hong, K. S., Sohn, H. C., and Hedrick, J. K., 2002, "Modified Skyhook Control of Semi-Active Suspensions: A New Model, Gain Scheduling, and Hardware-in-the-Loop Tuning," ASME J. Dyn. Syst. Meas. Control, **124**(1), pp. 158–167.
[33] Sammier, D., Sename, O., and Dugard, L., 2003, "Skyhook and H8 Control of Semi-Active Suspensions: Some Practical Aspects," Veh. Syst. Dyn., **39**(4), pp. 279–308.
[34] Silva, T. M. P., and De Marqui, C., Jr., 2016, "Energy Analysis of Semi-Passive Control for an Aeroelastic Plate-Like Wing Using Shunted Piezoelectric Materials," J. Intell. Mater. Syst. Struct., **27**(19), pp. 2599–2615.
[35] Chase, J. G., Mulligan, K. J., Gue, A., Alnot, T., Rodgers, G., Mander, J. B., and Heaton, D., 2006, "Re-Shaping Hysteretic Behaviour Using Semi-Active Resettable Device Dampers," Eng. Struct., **28**(10), pp. 1418–1429.
[36] Mulligan, K. J., Chase, J. G., Mander, J. B., Rodgers, G. W., Elliott, R. B., Franco-Anaya, R., and Carr, A. J., 2009, "Experimental Validation of Semi-Active Resettable Actuators in a $^1/_5$th Scale Test Structure," Earthquake Eng. Struct. Dyn., **38**(4), pp. 517–536.
[37] Guyomar, D., Richard, C., Gehin, C., and Audigier, D., 2000, "Low Consumption Damping of Planar Structures," 12th IEEE International Symposium on Applications of Ferroelectrics (ISAF), Honolulu, HI, July 21–Aug. 2, pp. 761–764.
[38] Guyomar, D., Badel, A., Lefeuvre, E., and Richard, C., 2005, "Toward Energy Harvesting Using Active Materials and Conversion Improvement by Nonlinear Processing," IEEE Trans. Ultrason., Ferroelectr. Freq. Control, **52**(4), pp. 584–595.
[39] Lefeuvre, E., Badel, A., Petit, L., Richard, C., and Guyomar, D., 2006, "Semi-Passive Piezoelectric Structural Damping by Synchronized Switching on Voltage Sources," J. Intell. Mater. Syst. Struct., **17**(8–9), pp. 653–660.
[40] Erturk, A., and Inman, D. J., 2008, "A Distributed Parameter Electromechanical Model for Cantilevered Piezoelectric Energy Harvesters," ASME J. Vib. Acoust., **130**(4), p. 041002.
[41] Lallart, M., Lefeuvre, E., Richard, C., and Guyomar, D., 2008, "Self-Powered Circuit for Broadband, Multimodal Piezoelectric Vibration Control," Sens. Actuators A, **143**(2), pp. 377–382.
[42] Petit, L., Lefeuvre, E., Richard, C., and Guyomar, D., 2004, "A Broadband Semi Passive Piezoelectric Technique for Structural Damping," Proc. SPIE, **5386**, pp. 414–425.